Applied Catalysis B: Environmental 136–137 (2013) 48–55

Contents lists available at SciVerse ScienceDirect

Applied Catalysis B: Environmental

journal homepage: www.elsevier.com/locate/apcatb

Aluminumphosphate molecular sieves supported Pt–Co catalysts for the preferential oxidation of CO in H_2-rich gases

ChangXu Wang, Lihong Zhang, Yutan Liu*

Tianjin Key Laboratory of Applied Catalysis Science and Engineering, Department of Catalysis Science and Technology, School of Chemical Engineering, Tianjin University, Tianjin 300072, China

ARTICLE INFO

Article history:
Received 5 July 2012
Received in revised form 30 January 2013
Accepted 1 February 2013
Available online 11 February 2013

Keywords:
Aluminophosphate
AlPOs
Preferential oxidation
Platinum
Cobalt

ABSTRACT

A series of aluminumphosphate molecular sieves supported platinum–cobalt catalysts were prepared and tested for the preferential oxidation of CO in H_2-rich gases. The catalysts were characterized by XRD, HRTEM, EDX, TPR and XPS techniques. The optimized catalysts were highly active and selective, CO could be purified below 10 ppm in the reaction temperature range of 110 °C–125 °C under 1% CO, 1% O_2, 12.5% CO_2, 15% H_2O, 50% H_2 in volume and N_2 balance at the space velocity of 24,000 mL g_{cat}^{-1} h^{-1}. Pt–Co/CoAPO-5 exhibited the best catalytic performance and Pt–Co/AlPO-5 was the most active catalyst at low reaction temperature, in which particles of Pt–Co alloy were formed and the particles were highly dispersed on the surface of the support. The high activity could be attributed to the Pt–Co nano-partilces with small sizes. The enlarged temperature window for CO purification should be ascribed to the loaded cobalt oxide. Substitution of cobalt ions for aluminium ions has obvious influence on the interaction between the support and platinum/cobalt species.

1. Introduction

The hydrogen for fuel cells such as polymer exchange membrance fuel cell (PEMFC) is usually generated by reforming of hydrocarbon followed by water-gas-shift (WGS) process. The resulted H_2-rich gases contain approximately 0.5–2.0 vol.% CO, which would poison the anodic Pt electrode of PEMFC [1]. Thus, CO should be eliminated below 100 ppm before use. Among the CO removing methods, the preferential oxidation (PROX) of CO is regarded as one of the most promising ways.

So far, catalysts for CO-PROX reported include noble metal catalysts [2], such as Pt [3], Pd [4], Rh [5] and Au [6] and base metal catalysts [7], such as CuO/CeO_2 [8], cobalt oxide [9–11], $LaCoO_3$ with perovskite structure [12] and copper–manganese mixed oxide [13]. The base metal catalysts are cheap and highly active, while improvement on stability is needed. The Pt-based catalysts usually show good activity only at the high temperature above 150 °C [14,15]. The supported gold catalysts are reported to be very active for the PROX at low temperature, but the selectivity for CO oxidation decreases quickly at high temperature [15]. The Ru-based catalysts are recognized as the most active catalysts by Djinovic and his co-authors. However the CO methanation, which consumes hydrogen, becomes dominated at high reaction temperatures [16].

Pt-based catalysts modified with base metal, such as Co, Ni, Fe or Sn, usually show improved catalytic performance, which is mainly owing to the formation of the base metal–platinum alloy. The support also has a marked influence on the modified Pt-based catalysts. The effects of various supports have been studied, including SiO_2 [17], CeO_2 [18], Nb_2O_5 [3], carbon nanotube [19,20] and zeolite. As for Pt–Co catalysts, supports of γ-Al_2O_3 [21], TiO_2 [22], silica aerogel [23] and yttria-stabilized zirconia (YSZ) [24] have been studied. Some supports could help to distribute the active component uniformly [19], some could interact with the active component [5] or influence the chemical state of the active component [25].

Recently, zeolite as support for CO-PROX catalyst has attracted attention. Its uniform micropores and large surface area could help the supported active species to be much highly dispersed. The zeolite supported platinum catalyst could give high activity at low reaction temperature. The reported zeolites as the supports for CO-PROX include ZSM-5 [26], zeolite Y [27], titanosilicates (ETS-10) [27], A-zeolites [29], FSM-16[30] and mordenite [31,32].

Aluminophosphate molecular sieves (AlPOs) [33] have attracted a lot of interest in recent years. AlPO is a type of molecular sieve composed of aluminum-oxygen tetrahedron and phosphorus-oxygen tetrahedron. AlPO-5 is one of the most frequently studied AlPOs, which has one-dimensional micropore structure composed of 4, 6 and 12 ring straight channels. Aluminium ions in AlPO-5 could be partially substituted by some other transition metal ions, such as cobalt, manganese, nickel and platinum ions. The substituted AlPO-5 is generally signed as MeAPO-5, where the Me

* Corresponding author. Tel.: +86 02287401675.
E-mail address: yuanliu@tju.edu.cn (Y. Liu).

0926-3373/$ – see front matter © 2013 Elsevier B.V. All rights reserved.
http://dx.doi.org/10.1016/j.apcatb.2013.02.001

stands for the substitution metal element. It was reported that MeAPO-5 showed good activity for some oxidation reaction, for example, selective oxidation of cyclohexane by N_2O [34,35].

Different from the well studied aluminosilicate zeolites, AlPO-5 containing phosphor and the aluminium ions could be partially replaced by some transitional metal ions. Thus, it is of interest to know the catalytic behavior of AlPO-5 supported Pt-based catalyst for CO-PROX and the effect of substitution of metal ions. However, to the best of our knowledge, no research about AlPOs used in CO-PROX has been reported.

Here a series of AlPO-5 and CoAPO-5 supported Pt–Co catalysts were prepared and investigated for CO-PROX reaction to study the effect of the support and the cobalt substitution for aluminium on the catalytic performance and on the catalyst structure. The results show that the prepared catalysts are highly active and selective for CO-PROX.

2. Experimental

2.1. Preparation of catalysts

Samples of AlPO-5 were prepared according to the method stated in the literature [33]. The zeolites were prepared by direct hydrothermal synthesis. Triethylamine (TEA) was used as the template. The solution of phosphoric acid (85 wt %) was added into a pseudo-boehmite sol under violent stirring, maintained the stirring for 3 h to got a uniform sol. Then, the template was added dropwise into the sol under vigorous stirring, making a mixture with molar ratio of Al_2O_3:P_2O_5:TEA:H_2O = 1:1:1.4:40. After stirring for 4 h, the resulting homogeneous gel was transferred into a stainless-steel autoclave with its inner surface coated with Teflon, and was kept at 200 °C for several hours. It was then cooled and washed with deionized water, dried at 110 °C for 3 h, calcined at 550 °C for 6 h.

Samples of CoAPO-5 were prepared according to the same method with the molar ratio of Al_2O_3:P_2O_5:TEA:Co:H_2O = 1:1:1.4:0.1:40. Cobalt nitrate was used as the cobalt source, and it was added into the sol together with phosphoric acid.

The supported Pt catalysts were prepared by using incipient wetness impregnation method. The amount of the platinum loading was 1.0% in weight, which is platinum metal in the calcined catalyst. The support of AlPO-5, CoAPO-5 or Al_2O_3 was impregnated with chloroplatinic acid ($H_2PtCl_6{\cdot}6H_2O$) and it was treated with ultrasound for 1 h. Then it was dried at 110 °C for 3 h and calcined at 500 °C for 3 h.

The supported Pt–Co catalysts were prepared according to co-impregnation method with cobalt nitrate as the precursor. The other conditions were the same to that of the supported Pt catalysts. The amount of cobalt loading was 2.0% in weight which is cobalt metal in the calcined catalyst.

2.2. Catalyst characterizations

X-ray diffraction (XRD) tests were performed on a Rigaku D/max 2500 v/Pc X-ray diffractometer with Ni filtered Cu-Ka radiation (λ = 0.15406 nm, 40 kV, 200 mA). The XRD patterns were recorded in the 2θ range of 3–55°, with a scan speed of 4°/min.

Transmission electron microscopy (TEM) pictures were obtained on a Tecnai G^2 F20 micro-scope operated at 200 kV. Samples were finely grounded in a mortar to fine particles and dispersed ultrasonically in ethanol. The well dispersed samples were deposited on a grid covered by a carbon film for measurements. The energy-dispersive X-ray spectroscopy (EDX) was performed along with observation of TEM. The particle size distribution was derived according to the equalize method, about 50 particles were counted and used to calculate the arithmetic mean value. The catalysts were reduced before TEM tests at 300 °C for 1 h in the gas mixture of 50 vol.% H_2 in N_2.

Temperature-programmed reduction (TPR) tests were performed under 5% H_2 in Ar at a flow rate of 30 mL min^{-1} with a heating rate of 10 °C min^{-1}. 50 mg of sample was used for each test.

X-ray photoelectron spectroscopy (XPS) experiments were performed using PERKIN ELMER PHI 1600 spectrometer equipped with a Mg Ka source at a beam power of 250 W. Extended spectra (survey) were collected in the range of 0–1350 eV (187.85 eV pass energy). The binding energy (BE) was calibrated with a reference of the C1s photoelectron peak located at 284.6 eV which was the adventitious carbon.

Brunauer–Emmett–Teller (BET) specific surface areas were obtained at 77 k on an Autosorb-1 equipment with N_2 physical adsorption.

2.3. Catalytic performance test

Catalytic performance tests were carried out on a continuous flow fixed tubular quartz micro-reactor with the inner diameter of 8 mm under atmospheric pressure. In each test, the catalysts were pre-reduced at 300 °C for 1 h with 50 vol.% H_2 in N_2 .The reaction gas mixture was consisted of 1 vol.% CO, 1 vol.% O_2 and 50 vol.% H_2 with N_2 balance. For investigating the influence of CO_2 and H_2O, 12.5 vol.% CO_2 and 15 vol.% H_2O was added into the reaction gas mixture, respectively. The total flow rate was 40 mL min^{-1}. CO conversion and selectivity were obtained under steady reaction state. At each testing temperature, reaction was carried through for more than 25 min. The reaction temperature was monitored by a K-type thermocouple placed in the catalysts and controlled by a temperature controller. The effluent gases were analyzed using an on-line gas chromatograph (GC) of SP-3420 equipped with a TCD and a column packed with 5A molecular sieve. As for detecting the CO concentration at ppm level, FID was used as the detector and equipped with a methanator, thus the CO detection limit was 1 ppm. The activities were evaluated on the basis of CO conversion, which can be calculated on the basis of CO in the reactant gas and the effluent gas. The selectivity of O_2 for CO oxidation is defined as the ratio of O_2 consumption for the CO oxidation to total O_2 consumption. The following are the formulae.

$$X_{CO} = \frac{[CO]_{in} - [CO]_{out}}{[CO]_{in}} \times 100$$

$$S_{O_2} = \frac{[CO]_{in} - [CO]_{out} - [CH_4]_{out}}{2 \times ([O_2]_{in} - [O_2]_{out})} \times 100$$

3. Results and discussion

3.1. Catalytic performance

Fig. 1 shows the CO conversion and the selectivity of O_2 for CO oxidation over AlPO-5 zeolite supported Pt–Co catalysts. Pure AlPO-5 and CoAPO-5 showed poor activity, CO conversions were lower than 10% at 170 °C, which were not shown here. Co/CoAPO-5 was a little more active than CoAPO-5, but its activity was still poor, CO conversion was 84% at the high temperature of 200 °C, as could be seen from Fig. 1. This indicated that cobalt species added by impregnation performed a better activity than that of cobalt species in the crystalline lattice of CoAPO-5. Cobalt ions added by impregnation were on the surface of CoAPO-5, i.e. outside the framework of the zeolite, which could be seen from the characterization results below.

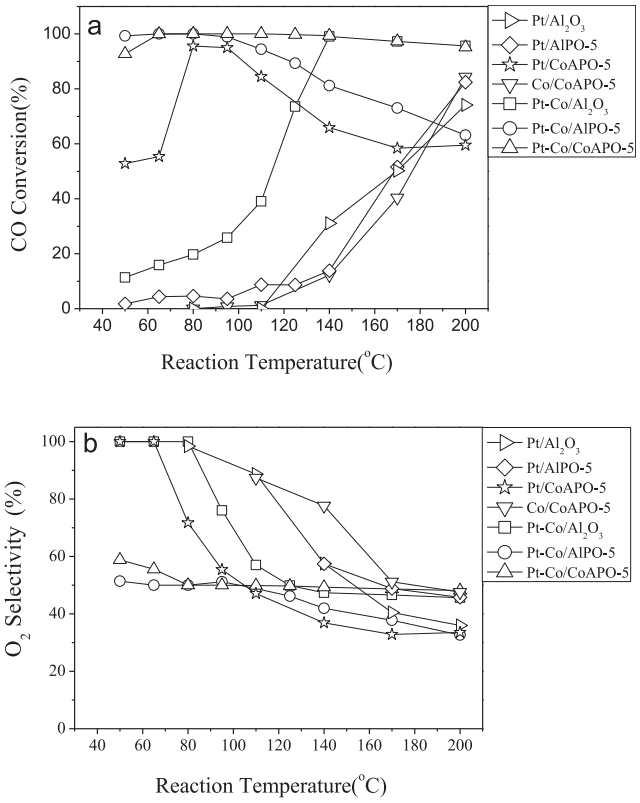

Fig. 1. Variation of CO conversion (a) and the selectivity of O_2 for CO oxidation (b) with reaction temperature over catalysts of in the reaction gas mixture of 1 vol.% CO, 1 vol.%O_2, 50 vol.% H_2 and N_2 balance under space velocity of 24,000 mL g_{cat}^{-1} h^{-1}.

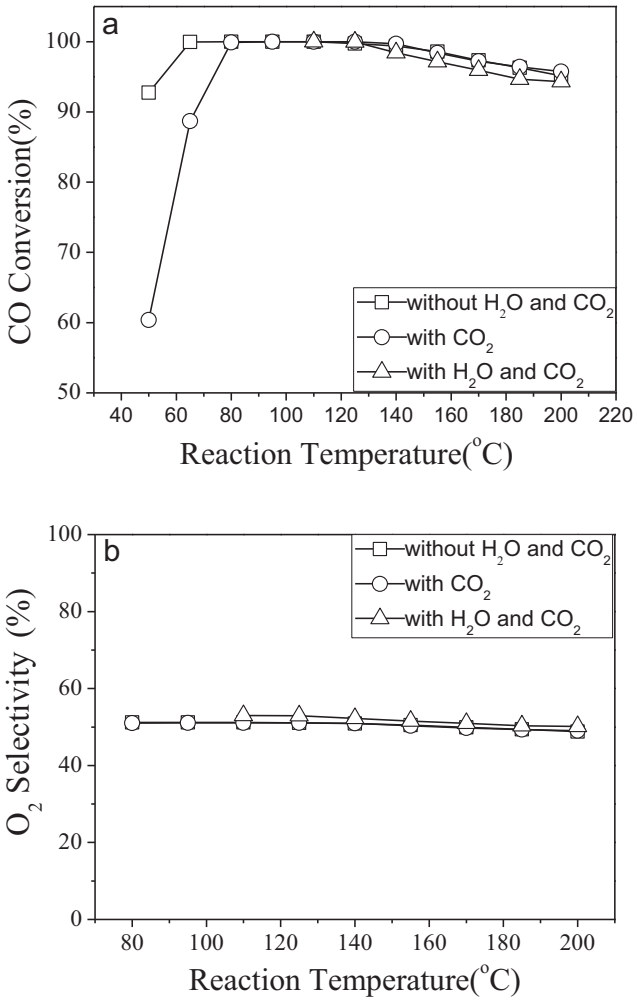

Fig. 2. Effects of H_2O and CO_2 in feeding gas over Pt–Co/CoAPO-5 on CO conversion (a) and the selectivity (b) in reaction gases of 1 vol % CO, 1 vol.% O_2, 0–2.5 vol % CO_2, 0–15 vol.% H_2O, 50 vol.% H_2 and N_2 balance at space velocity of 24,000 mL g_{cat}^{-1} h^{-1}.

Pt/Al_2O_3 and Pt/AlPO-5 showed very weak activity, CO conversion was negligible below 140 °C and increased to 74% and 82.5% at 200 °C, respectively. By comparison, Pt/CoAPO-5 catalyst showed a much better activity with CO conversion of about 95% in the temperature range of 85–95 °C. This suggested that cobalt ions in AlPO-5 crystalline had marked influence on the catalytic performance of the supported platinum.

$Pt–Co/Al_2O_3$ showed a poor activity as the reaction temperature was lower than 120 °C. CO conversion increased with increasing reaction temperature in the temperature range of 50–140 °C and reached 100% at 140 °C. The catalytic performance of $Pt–Co/Al_2O_3$ was close to that of the catalyst with the same composition reported in literatures [36]. It was reported that cobalt modification could improve the activity of Pt-based catalysts for CO-PROX. Komatsu and Tamura [37] ascribed the improvement to the formation of Pt_3Co alloy. More detailed mechanism had been proposed for the doping of transitional metals, such as cobalt, nickel and iron. The single Pt activates O_2 not well, due to that the surface is covered by the strongly adsorbed CO. For bimetallic catalysts, such as Pt–Fe, Watanabe and co-workers [38] pointed that CO was adsorbed on the Pt sites and O_2 was dissociated on the Fe sites. The CO oxidation reaction took place at the boundary between the platinum and the iron.

Compared with $Pt–Co/Al_2O_3$, Pt–Co/AlPO-5 and Pt–Co/CoAPO-5 were much more active. Over Pt–Co/APO-5, complete CO conversion was observed in the range of 65 °C–80 °C. Pt–Co/CoAPO-5 showed wide temperature window for purifying CO from the H_2-rich gases, the complete CO conversion temperature range was 65 °C–110 °C; the temperature range for CO conversion of above 99%, corresponding to 100 ppm of CO in the reacted gas mixtures, was 65 °C–140 °C. It had been reported that zeolite supported Pt-based catalyst exhibited better activity than that of alumina supported Pt-based catalyst. Kotobukis et al. [21,39] prepared Pt–Fe/mordenite catalysts and found it showed better activity than that of Pt–Fe/alumina. The reason was ascribed to that the adsorption property of CO and O_2 was influenced by the zeolite cages. Some authors focused on the molecular sieve effect and tried to write an order of the activity for Pt loaded catalysts as follows: A-type zeolite > mordenite > X-type zeolite > alumina [32,40]. AlPOs was not included in that sequence, for that AlPOs used in CO-PROX had not been reported.

The Pt–Co/CoAPO-5 catalyst showed the most interesting character. It had a better selectivity than Pt–Co/AlPO-5 at the reaction temperature of over 80 °C. The reasons will be discussed below.

Generally, the H_2-rich gases from hydrocarbon reforming contained 10-20 vol.% CO_2 and 10-20 vol.% H_2O. Fig. 2 shows the influence of H_2O and CO_2 on the CO conversion. CO_2 had a slight negative effect on CO conversion over Pt–Co/CoAPO-5, the temperature range for complete CO conversion was put off by about 15 °C. Adding water in the gas led to a slight decrease of the conversion. In reaction gas mixtures which containing both of H_2O and CO_2, complete CO conversion was obtained at 110 °C and CO conversion of above 99.9% was obtained in the range of 110 °C–125 °C over the catalyst. CO conversion of 99.9% was corresponding to 10 ppm of CO in the reacted gases.

The slight negative effect of CO_2 on CO conversion at low temperatures might be ascribed to the adsorption of CO_2 on the active

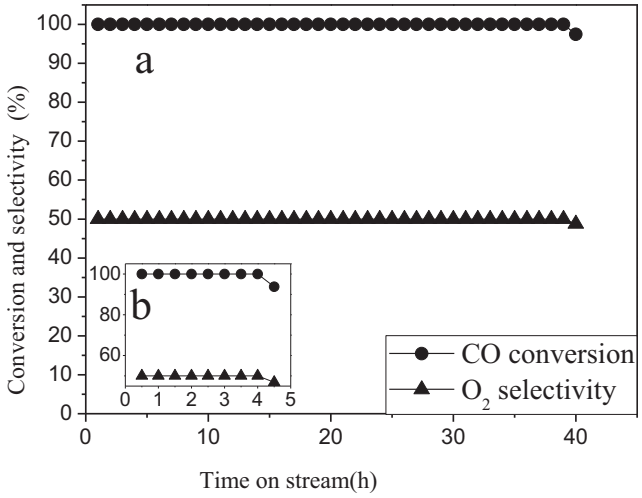

Fig. 3. Stability of Pt–Co/CoAPO-5 in the reaction gases of 1 vol.% CO, 1 vol.%O_2, 50 vol.% H_2 and N_2 balance at 80 °C (a) and in the gas of 1 vol % CO, 1 vol.% O_2, 12.5 vol % CO_2, 15 vol.% H_2O, 50 vol.% H_2 and N_2 balance at 110 °C (b). The space velocity is 24,000 mL g_{cat}^{-1} h^{-1}.

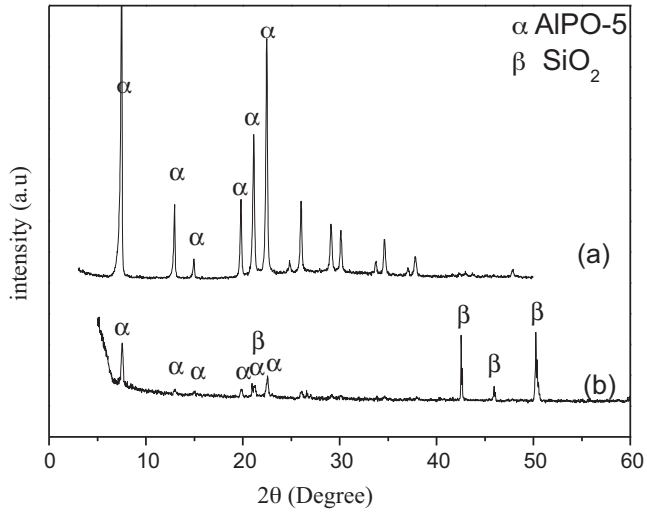

Fig. 5. XRD patterns of Pt–Co/CoAPO-5 (a) fresh and (b) used in water and CO_2 containing reaction mixtures, the detail reaction conditions were the same as Fig. 2.

sites for activating oxygen. When the reaction temperature was higher than 80 °C, the negative effect of CO_2 was negligible. Luengnaruemitchai et al. [40] had reported CO_2 could even improve the activity on Pt/A-type catalyst and pointed that over the zeolite of LTA, CO_2 could inhibit the generation of the reverse WGS reaction. The reverse WGS reaction produces CO and thus hinders the purification of CO. This might not be fit for this case. According to the thermodynamics analysis [41], reverse WGS reaction could not take place at the low reaction temperature of this study, which was an endothermic reaction.

The slight negative effect of water on CO conversion might be due to the adsorption of water on the support which blocked parts of the micropores of the zeolite support, as stated by Maeda [42]. He suggested that when zeolite-supported catalysts were used at a low temperature, the "flooding" of the nano-pores with water was generally a matter of concern.

The results of the stability tests for Pt–Co/CoAPO-5 catalyst with different reaction gases are shown in Fig. 3. In the gases of 1 vol.% CO, 1 vol.%O_2, 50 vol.% H_2 and N_2 at a low reaction temperature of 80 °C, complete conversion of CO maintained for 39 h. As adding 12.5 vol % CO_2 and 15 vol.% H_2O into the reaction mixture and at 110 °C, complete conversion of CO maintained only 4 h. The results indicate that the catalyst exhibit good stability at low reaction temperature, while the catalyst is not very stable in H_2O and CO_2 containing reaction mixture which may be mainly due to the interaction of CO_2 with the active species of cobalt. At temperature for the stability test of 110 °C, the activity was mainly attributed to the active sites of cobalt species (see discussions below), and CO_2 has an obvious effect on its stability. CO_2 can interact with cobalt ions and disturb the redox process of Co^{2+}/Co^{3+} which is important for CO oxidation [43].

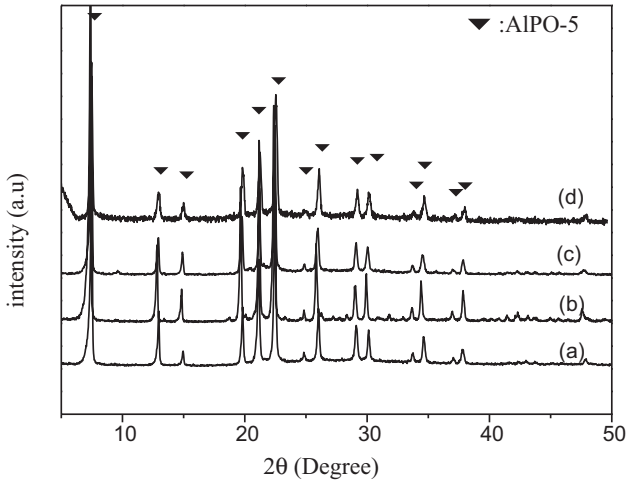

Fig. 4. XRD patterns of (a) AlPO-5, (b) Pt–Co/AlPO-5, (c) CoAPO-5 and (d) Pt–Co/CoAPO-5.

For comparison, the representative Pt–Co catalysts which exhibit excellent catalytic performance for CO-PROX reported in literatures are listed in Table 1. It is seen that AlPO-5 and CoAPO-5 supported Pt–Co are highly active at low reaction temperatures and can eliminate CO to ppm level in a wide temperature range in CO_2 and H_2O containing H_2-rich gases. AlPO-5 and CoAPO-5 supported Pt–Co are among the best catalysts for CO-PROX in the H_2-rich gases.

3.2. Catalyst characterization

3.2.1. XRD results and specific surface area

The XRD patterns of the catalysts are shown in Fig. 4. Three major peaks could be observed at 2θ of 7.4, 19.6 and 21.2°, which could be assigned to the lattice plane of (1 0 0), (2 1 0) and (0 0 2) of AlPO-5, respectively [27], confirming the formation of AlPO-5 type zeolite. Meanwhile, no peaks belonged to platinum and cobalt species could be observed, suggesting that Pt and CoO_x existed in highly dispersed or amorphous state.

A XRD pattern of the used catalyst is shown in Fig. 5. It can be seen that the catalyst still maintained the AlPO-5 structure. The diffraction peaks of the used AlPO are weaker, because that the used sample contained many quartz sands which were in the size close to the catalyst particles and hard to separate. The SiO_2 peaks are for the quartz sands which were mixed with the catalysts in the reaction. Considering the molecular sieve was treated in a higher temperature of 550 °C, the structure of AlPO-5 should be not destroyed in the reaction of CO-PROX. As the CoAPO-5 catalyst could be used in other more sever conditions [34,35], so the CoAPO-5 catalyst could be stable under the conditions of this work.

Specific surface areas of CoAPO-5 and Pt–Co/CoAPO-5 are listed in Table 2. The surface area of CoAPO-5 is 211 m^2 g^{-1}, in line with literature reports [28]. The surface area of Pt–Co/CoAPO-5 is reduced

Table 1
A comparison of catalytic performance for CO-PROX.

Catalyst	Temperature (K)[a]	GHVS (mL g_{cat}^{-1} h^{-1})	Feed composition in volume	Ref.
1%Pt–2% Co/Al_2O_3	413–453	10,910 h^{-1}	1% CO, 1.5%O_2, 50%H_2, 20% CO_2, 16.% H_2O and He balance	[44]
1.4%Pt–1.25%Co–1.25% Ce/MgO	423	24000	1% CO, 1% O_2, 60% H_2, 25% CO_2, 10% H_2O and He balance	[45]
5% Pt/FSM-16	333–423	12000	1% CO, 0.5% O_2, 5% H_2 and N_2 balance	[30]
0.5%Pt–5%Co/YSZ	380–423	16,680	0.9% CO, 0.9% O_2, 64.6% H_2, 17.4% CO_2,13% H_2O and N_2 balance	[24]
1%Pt–2%Co/AlPO-5	338–353	24,000	1% CO, 1% O_2, 50% H_2 and N_2 balance	This work
1%Pt–2%Co/CoAPO-5	338–383	24,000	1% CO, 1% O_2, 50% H_2 and N_2 balance	This work
1%Pt–2%Co/CoAPO-5	383–398	24,000	1% CO, 1% O_2, 50% H_2 15%H_2O 12.5% CO_2 and N_2 balance	This work

[a] This line refers to the temperature range of reducing CO concentration below 10 ppm

to 191 m^2 g^{-1}, this reduction should be attributed to the blockage of the micropores of the zeolite by the loaded nano particles.

3.2.2. TEM and EDX results and discussion

The TEM micrographs of the catalysts are shown in Fig. 6. The faint background belongs to zeolite support and the dark spots are platinum or Pt–Co particles. The distances of the crystal plane observed here are mainly of three kinds, that is, around 0.22 nm, 0.19 nm and 0.66 nm. 0.22 nm and 0.19 nm are corresponding to the (1 1 1) and (2 0 0) crystal planes of metal platinum or Pt–Co alloy, respectively, and 0.66 nm is the (1 1 0) crystal plane of AlPO-5. It should be mentioned here that no crystal planes of cobalt oxide were observed .This is probably because that cobalt species were highly dispersed and interacted with platinum or they existed in amorphous state. Fu and his co-workers [22] reported a Pt/Co–B catalyst and pointed out that the Co–B components exist as an amorphous structure. After reduction, particles of Pt–Co alloy were formed, which will be discussed below.

The platinum or Pt–Co particles on the supports showed a uniform distribution and small particle sizes. The average particle size was 1.6 nm for Pt in Pt/AlPO-5 and 2.1 nm for Pt–Co in Pt–Co/AlPO-5. However, the size of the particles on CoAPO-5 support was obviously bigger; which was 4.5 nm for Pt in Pt/CoAPO-5 and 5.5 nm for Pt–Co in Pt–Co/CoAPO-5, indicating that the interaction between the particles of Pt and Pt–Co with CoAPO-5 was weaker than that of with AlPO-5. The weaker interaction resulted in aggregation of the supported particles which led to a higher size of the particles.

The TEM and corresponding EDX results are shown in Fig. 7. Pt–Co particles on AlPO-5 and CoAPO-5 are exhibited in Fig. 7A and B, respectively. EDX tests were carried out inside the circles signed in Fig. 7. It can be seen that platinum species coexisted with cobalt species in both of the cases, suggesting the formation of Pt–Co alloy. It was generally accepted that the Pt–Co alloy accounted for the high activity for CO-PROX. For example, Yu [46] and Komatsu [36] studied the Pt–Co alloy catalysts pointed out the synergistic effect in the bimetal catalysts of Pt–Co.

3.2.3. TPR and XPS results

The TPR profiles of the catalysts with different supports are shown in Fig. 8. AlPO-5 did not show evident peaks, so it was not shown here. CoAPO-5 exhibited a broad and weak peak in the range of 100 °C–400 °C, which could be due to the reduction of hydroxyl groups [47]. Pt/AlPO-5 catalyst showed two reduction peaks, which was similar to other Pt/zeolites catalysts [27]. The peak at the lower temperature was attributed to the reduction of surface platinum ions and the broad peak at the higher temperature was related to the reduction of Pt ions at the ion-exchange sites. Likely, Pt/CoAPO-5 exhibited two reduction peaks; the attribution of the peaks was like that for Pt/AlPO-5.

As for the bimetal catalysts, two reduction peaks can be observed and signed as α and β. The peaks of α belonged to the reduction of Pt–Co cluster to form Pt–Co alloy particles. The peaks of β were due to the reduction of supported cobalt ions [24,48]. The hydrogen consumption corresponding to α peaks for Pt–Co/AlPO-5 and Pt–Co/CoAPO-5 was obviously higher than the hydrogen consumption corresponding to the reduction of platinum ions for Pt/AlPO-5 and Pt/CoAPO-5, which was an indication for the formation of Pt–Co alloy in Pt–Co/AlPO-5 and Pt–Co/CoAPO-5 [24,48].

The reduction temperature for Pt/CoAPO-5 was obviously lower, as to compare the peaks corresponding to the reduction of Pt ions at the ion-exchange sites in Pt/AlPO-5 and Pt/CoAPO-5, to see the broad peaks at higher temperature of curve (b) and (c) in Fig. 8. It was recognized that weaker interaction between platinum and its support would lead to a lower reduction temperature of the supported platinum ions [27]. Thus, the partial substitution of cobalt ions for aluminium ions weakened the interaction between platinum and AlPO-5 support.

To compare the peaks of the reduction of the cobalt ions in Pt–Co/AlPO-5 and Pt–Co/CoAPO-5, which were β peaks in curve (d) and (e) in Fig. 8, the reduction temperature for Pt–Co/CoAPO-5 was lower. This means that the partial substitution of cobalt ions for aluminium ions has effect on the interaction between cobalt ions and AlPO-5 support, which results in the easier reduction of the supported cobalt ions.

The surface composition derived from XPS characterization is listed in Table 2. For Pt/CoAPO-5, signals of Co2p could hardly be seen, demonstrating that cobalt ions were distributed in the lattice of the zeolite and not enriched on the surface. Compared with Pt–Co/Al_2O_3 and Pt–Co/AlPO-5, It can be seen that the cobalt substitution led to the enrichment of the impregnated cobalt species on the support surface.

To summarize the characterization results, the following conclusions could be drawn. Platinum and cobalt species could be highly dispersed on AlPO-5 and CoAPO-5 surface and nanoparticles of Pt–Co alloy were formed by using the simple impregnation method. Substitution cobalt ions for aluminium ions had obvious influence on the interaction between the supported metal and AlPO-5 support. As the results, for the CoAPO-5 supported catalysts, the interaction between platinum species and the support was weakened, the size of the nano-particles of the supported Pt and Pt–Co increased and the reduction temperature of the supported cobalt species lowered

Table 2
the molar ratios of Co/Al on the surface of catalyst and derived from XPS results and the specific surface areas.

	CoAPO-5	Pt/CoAPO-5	Pt–Co/Al_2O_3	Pt–Co/AlPO-5	Pt–Co/CoAPO-5
Molar ratio Co/Al	–	0.	0.03	0.26	0.56
Surface area (m^2 g^{-1})	211	–	–	–	191

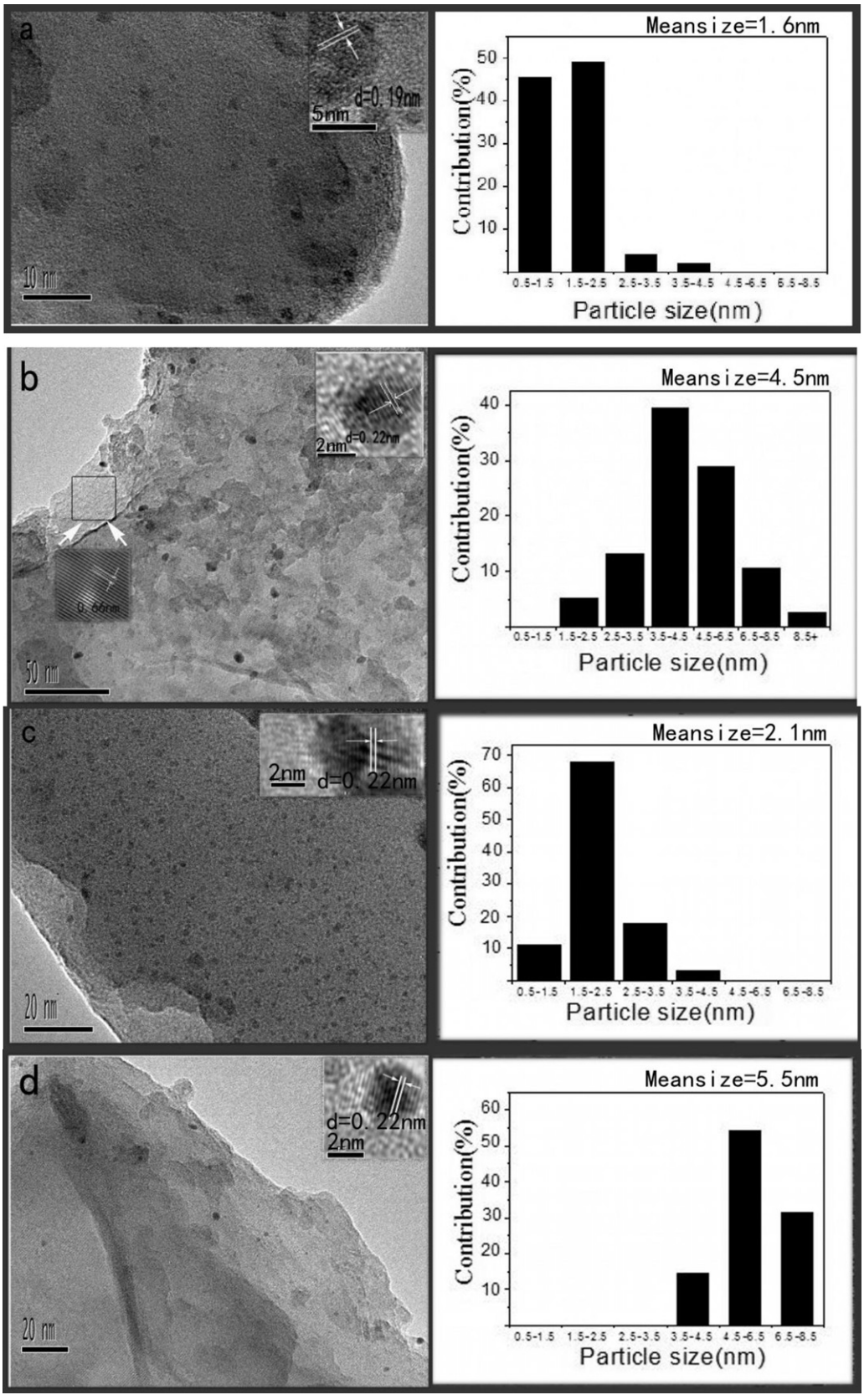

Fig. 6. TEM images of (a) Pt/AlPO-5, (b) Pt/CoAPO-5, (c) Pt–Co/AlPO-5 and (d) Pt–Co/CoAPO-5.

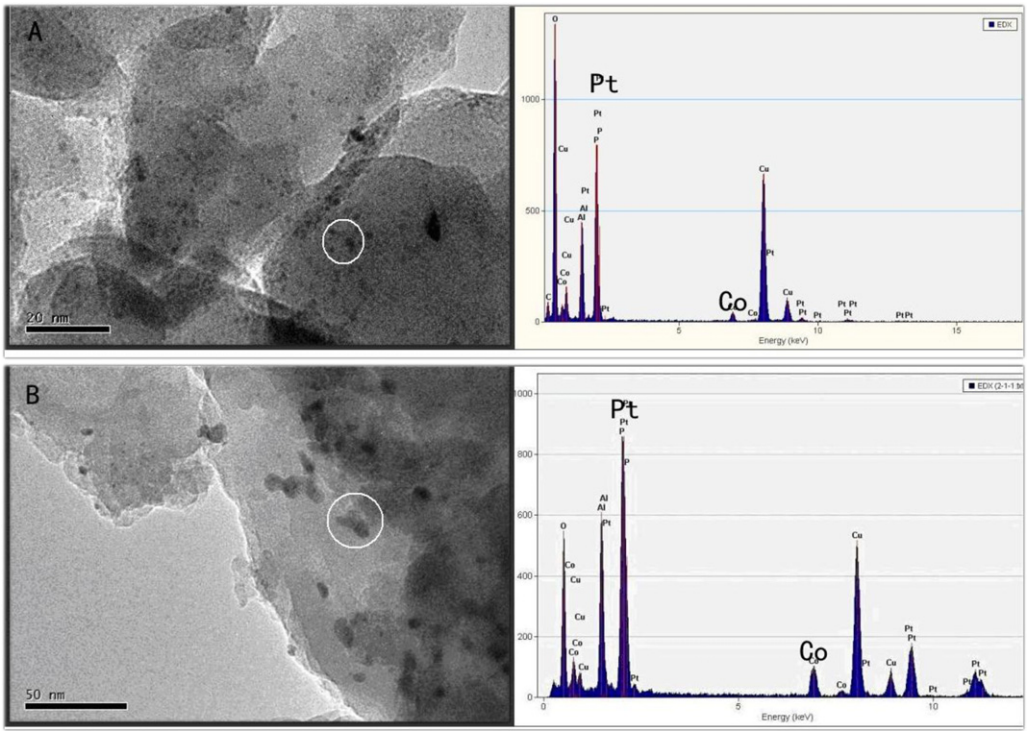

Fig. 7. TEM micrographs and corresponding EDX results of (A) Pt–Co/AlPO-5 and (B) Pt–Co/CoAPO-5.

It was known that both of single cobalt oxide and supported cobalt oxide were active for CO oxidation and CO-PROX reactions [49–51]. The activity of cobalt oxide for CO oxidation was ascribed to its redox property [52,53], meaning that cobalt species which inclined to be reduced and then be re-oxidized could show good activity. In this process, the oxidizing of the cobalt species related to the adsorption and activation of oxygen, which was a facile step. The reduction was generally the controlling step [10,54]. Hence, the reduction behavior was important for its activity of CO oxidation.

Comparing the catalytic performance of Pt–Co/CoAPO-5 with that of Pt–Co/AlPO-5, the former exhibited much higher CO conversion (Fig. 1) at reaction temperatures of above 80 °C. Comparing the TPR curves of the two catalysts (Fig. 8), the reduction peak of cobalt oxide on the CoAPO-5 is at around 150 °C, while that on AlPO-5 is around 220 °C. Correlating the TPR results with the catalytic performance, the higher CO conversion over Pt–Co/CoAPO-5 at above 80 °C is attributed to the cobalt oxide supported on CoAPO-5.

As reaction temperature is lower than 80 °C, Pt–Co/AlPO-5 is more active than Pt–Co/CoAPO-5 (Fig. 1), which should be owing to the smaller size of Pt–Co particles in Pt–Co/AlPO-5 (Fig. 6).

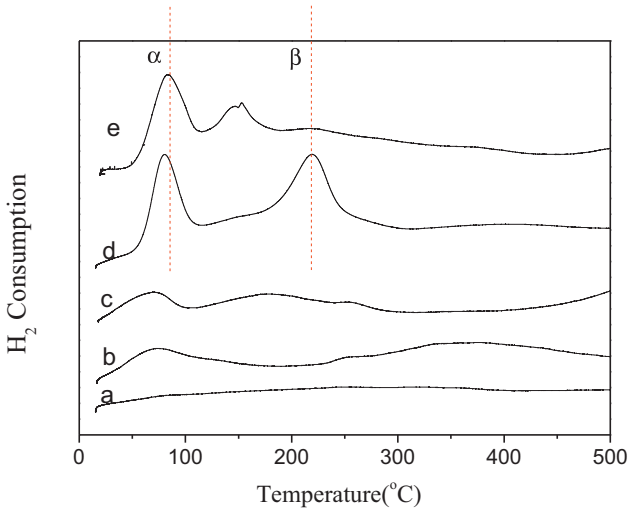

Fig. 8. TPR profiles of (a) CoAPO-5, (b) Pt/AlPO-5, (c) Pt/CoAPO-5, (d) Pt–Co/AlPO-5 and (e) Pt–Co/CoAPO-5.

4. Conclusions

AlPO-5 and CoAPO-5 supported Pt–Co catalysts were highly active and selective for CO-PROX in H_2-rich gases, which are among the best active catalysts reported till now. The high activity at the low temperature should be attributed to the formation of Pt–Co alloy particles with nanometer size. The loaded cobalt species on CoAPO-5 were proposed to be active at the comparatively high temperature, which had enlarged the temperature window for purifying CO from the H_2-rich gases. Replacing aluminium ions partially with cobalt ions in AlPO-5 obviously affected the interaction between the supported metal and AlPO-5, which weakened the interaction between platinum species and the AlPO-5 support, led to the supported nano-particles of Pt and Pt–Co tending to congregate, and favored the reduction of the supported cobalt ions.

Acknowledgements

Financial support from the NSF of China (Nos. 20976121, 20901056), the NSF of Tianjin of China (10JCZDJC23800) and Doctoral Fund of Ministry of Education of China (20100032110019) are gratefully acknowledged.

References

[1] E.D. Park, D. Lee, H.C. Lee, Catalysis Today 139 (2009) 280–290.
[2] K. Liu, A. Wang, T. Zhang, Advanced synthesis and Catalysis 2 (2012) 1165–1178.
[3] T.S. Mozer, F.B. Passos, International Journal of Hydrogen Energy 36 (2011) 13369–13378.
[4] A. Parinyaswan, S. Pongstabodee, A. Luengnaruemitchai, International Journal of Hydrogen Energy 31 (2006) 1942–1949.

[5] Y.H. Kim, E.D. Park, H.C. Lee, D. Lee, K.H. Lee, Catalysis Today 146 (2009) 53–259.
[6] Y.B. Tu, J.Y. Luo, M. Meng, G. Wang, J.J. He, International Journal of Hydrogen Energy 34 (2009) 3743–3754.
[7] A. Mishra, R. Prasad, Bulletin of Chemical Reaction Engineering Catalysis (2011).
[8] C.L. Gu, S.H. Lu, J. Miao, Y. Liu, Y.Q. Wang, International Journal of Hydrogen Energy 35 (2010) 6113–6122.
[9] Q. Guo, Y. Liu, Applied Catalysis B: Environmental 82 (2008) 19–26.
[10] Z. Zhao, X. Lin, R. Jin, G. Wang, T. Muhammad, Applied Catalysis B: Environmental 115–116 (2012) 53–62.
[11] T. Bao, Z. Zhao, Y. Dai, X. Lin, R. Jin, G. Wang, T. Muhammad, Applied Catalysis B: Environmental 119–120 (2012) 62–73.
[12] C.A. Chagas, F.S. Toniolo, R.N.S.H. Magalhães, M. Schmal, International Journal of Hydrogen Energy 37 (2012) 5022–5031.
[13] J. Papavasiliou, G. Avgouropoulos, T. Ioanides, Applied Catalysis B: Environmental 66 (2006) 168–174.
[14] A. Manasilp, E. Gulari, Applied Catalysis B: Environmental 37 (2002) 17–25.
[15] S.L. Zhou, Z.S. Yuan, S.D. Wang, International Journal of Hydrogen Energy 31 (2006) 924–933.
[16] P. Djinovic, C. Galletti, S. Specchia, V. Specchia, Catalysis Today 164 (2011) 282–287.
[17] M.M.V.M. Souza, N.F.P. Ribeiro, M. Schmal, International Journal of Hydrogen Energy 32 (2007) 425–429.
[18] J.L. Ayastuy, A. Gil-Rodriguez, M.P. Gonzalez-Marcos, M.A. Gutierrez-Ortiz, International Journal of Hydrogen Energy 31 (2006) 2231–2242.
[19] S.H. Lu, C. Zhang, Y. Liu, International Journal of Hydrogen Energy 36 (2011) 1939–1948.
[20] S.H. Lu, Y. Liu, Applied Catalysis B: Environmental 111–112 (2012) 492–501.
[21] C. Kwak, T.J. Park, D.J. Suh, Applied Catalysis A: General 278 (2005) 181–186.
[22] Z.X. Ding, H.Y. Yang, J.F. Liu, W.X. Dai, X. Chen, X.X. Wang, X.Z. Fu, Applied Catalysis B: Environmental 101 (2011) 326–332.
[23] J. Choi, C.B. Shin, D.J. Suh, Catalysis Communications 9 (2008) 880–885.
[24] E.Y. KO, E.D. Park, H.C. Lee, D. Lee, S. Kim, Angewandte Chemie International Edition 46 (2007) 734–737.
[25] H.R. Zheng, H.Y. Yang, R.R. Si, W.X. Dai, X. Chen, X.X. Wang, P. Liu, X.Z. Fu, Applied Catalysis B: Environmental 105 (2011) 243–247.
[26] M. Kotobuki, A. Watanabe, H. Uchida, H. Yamashita, M. Watanabe, Chemistry Letters 34 (2005) 866–867.
[27] V. Sebastian, S. Irusta, R. Mallada, J. Santamaria, Applied Catalysis A: General 366 (2009) 242–251.
[28] H. Shao, J. Yao, X. Ke, L. Zhang, N. Xu, Materials Research Bulletin 44 (2009) 956–959.
[29] I. Rosso, C. Galletti, G. Saracco, E. Garrone, V. Specchia, Applied Catalysis B: Environmental 48 (2004) 195–203.
[30] A. Fukuoka, J.I. Kimura, T. Oshio, Y. Sakamoto, M. Ichikawa, American Chemical Society 129 (2007) 10120–10125.
[31] M. Kotobuki, A. Watanabe, H. Uchida, H. Yamashita, Journal of Catalysis 236 (2005) 262–269.
[32] H. Igarashi, H. Uchida, M. Suzuki, Y. Sasaki, M. Watanabe, Applied Catalysis A: General 159 (1997) 159–169.
[33] J.H. Yu, R.R. Xu, Chemical Society Reviews 35 (2006) 593–604.
[34] R. Zhao, Y.Q. Wang, Y.L. Guo, Y. Guo, X.H. Liu, Z.G. Zhang, Y.S. Wang, W.C. Zhan, G.Z. Lu, Green Chemistry 8 (2006) 459–466.
[35] L.P. Zhou, J. Xu, H. Miao, X.Q. Li, F. Wang, Catalysis Letters 99 (2005) 231–234.
[36] C. kwak, T.J. Park, D.J. Suh, Applied Catalysis A: General 278 (2005) 181–186.
[37] T.M. Komatsu, A. Tamura, Journal of Catalysis 258 (2008) 306–314.
[38] M. Vishnuvarthan, V. Murugesan, E. Gianotti, L. Bertinetti, S. Coluccia, G. Berlieret, Microporous and Mesoporous Materials 123 (2009) 91–99.
[39] M. Kotobuki, A. Watanabe, H. Uchida, H. Yamashita, M. Watanabe, Applied Catalysis A: General 307 (2006) 275–283.
[40] A. Luengnaruemitchai, M. Nimsuk, P. Naknam, S. Wongkasemjit, S. Osuwan, International Journal of Hydrogen Energy 33 (2008) 206–213.
[41] D. Tibiletti, E.A.B. Graaf, S.P. Teh, G. Rothenberg, D. Farrusseng, C. Mirodatos, Journal of Catalysis 225 (2004) 489–497.
[42] N. Maeda, T. Matsushima, H. Uchida, H. Yamashita, M. Watanabe, Applied Catalysis A: General 341 (2008) 93–97.
[43] Q. Guo, Sh.Q. Chen, Y. Liu, Y.Q. Wang, Chemical Engineering Journal 165 (2010) 846–850.
[44] X.H. Yu, H.L. Li, S.T. Tu, J.J. Yan, Z.D. Wang, International Journal of Hydrogen Energy 36 (2011) 3778–3788.
[45] G. Uysal, A.N. Akin, I.O. Nsan, R. Yldrm, Catalysis Letters 108 (2006) 193–196.
[46] X.H. Yu, H.L. Li, S.T. Tu, J.Y. Yan, Z.D. Wang, International Journal of Hydrogen Energy 36 (2011) 3778–3788.
[47] B. Moden, L. Oliviero, J. Dakka, J.G. Santiesteban, E. Iglesia, Journal of Physical Chemistry B 108 (2004) 5552–5563.
[48] K.Y. Kim, S.W. Nam, J. Han, S.P. Yoon, T.H. Lim, H.I. Lee, Journal of Industrial and Engineering Chemistry 14 (2008) 853–859.
[49] H. Wang, H.Q. Zhu, Z.F. Qing, F.X. Liang, G.F. Wang, J.G. Wang, Journal of Catalysis 264 (2009) 154–162.
[50] F.B. Derekaya, Ç. Güldür, International Journal of Hydrogen Energy 25 (2010) 2247–2261.
[51] M.P. Woods, P. Gawade, B. Tan, U.S, Applied Catalysis B: Environmental 97 (2010) 28–35.
[52] X.W. Xie, Y. Li, Z.Q. Liu, M. Haruta, W. Shen, Nature 458 (2009) 746–749.
[53] A.V. Salker, S.J. Naik, Applied Catalysis B: Environmental 89 (2009) 246–254.
[54] S.H. Zeng, W.L. Zhang, S.L. Guo, H.Q. Su, Catalysis Communications 23 (2012) 62–66.